Nanoscale Horizons

ROYAL SOCIETY OF CHEMISTRY

COMMUNICATION

View Article Online
View Journal

Cite this: DOI: 10.1039/d5nh00855g

Received 31st December 2025,
Accepted 15th April 2026

DOI: 10.1039/d5nh00855g

rsc.li/nanoscale-horizons

STORM as a tool to track cargo release from polymeric nanocarriers at the single-particle level

Anna Solé-Porta, *[a] Silvia Pujals, *[b] Pietro Delcanale [c] and Anna Roig *[a]

Recent advances in super-resolution microscopy have enabled unprecedented visualization of cellular structures, tracking of nanomaterials in biological environments, or the elucidation of specific nano-bio interactions. Yet, dynamic quantification of cargo release from individual nanocarriers remains unexplored. Here, we leverage the high spatial resolution of direct stochastic optical reconstruction microscopy (dSTORM) to monitor protein release at the single-nanocarrier level. Poly(lactic-*co*-glycolic acid) (PLGA) nanocapsules labelled with Cyanine5 and loaded with bovine serum albumin (BSA) tagged with Alexa Fluor 488 are characterized using dSTORM alongside other characterization techniques. dSTORM allowed us to simultaneously observe changes in nanocarrier size and cargo localization over time. Our results demonstrate a time-dependent increase in nanocapsule diameter and a decrease in nanocarrier concentration. The quantitative analysis of individual nanocarriers reveals single-particle protein release profiles, characterized by an initial burst followed by sustained release, with complete release achieved after 30 days. This study represents the first application of super-resolution microscopy to spatially and temporally resolve protein release from nanocarriers, offering single-molecule sensitivity and nanometric resolution, and capturing heterogeneity that ensemble-averaged techniques overlook. Our approach complements other pharmacokinetic analyses and establishes a robust method to evaluate the cargo release from other nanocarriers by super-resolution microscopy.

New concepts

This work proposes super-resolution microscopy for resolving and quantifying drug release kinetics at the single-nanocarrier level. While super-resolution techniques have transformed our understanding of nano-bio interactions, their potential to dynamically monitor protein release from nanocarriers has remained unexplored. Here, we demonstrate the first application of direct stochastic optical reconstruction microscopy (dSTORM) to temporally and spatially track protein release from individual poly(lactic-*co*-glycolic acid) (PLGA) nanocapsules with nanometric precision. Unlike conventional bulk assays that provide ensemble-averaged release profiles, our MATLAB-based quantitative single-particle analysis captures nanocarrier heterogeneity and provide simultaneous information of the nanocarrier evolution over time and the protein release. This conceptual advance establishes dSTORM as a quantitative tool for studying cargo release from nanocarriers and intra-population variability, advancing the rational design and optimization of next-generation drug delivery systems.

1. Introduction

In recent years, nanocarriers have emerged as revolutionary tools in medical research, overcoming critical limitations of conventional free therapeutics. Nanocarriers can enhance the stability and solubility of encapsulated cargos, facilitate transport across biological membranes, and extend blood circulation times, thereby improving therapeutic efficacy while reducing off-target effects.[1,2] Owing to their versatility and customizability, polymeric nanocarriers have garnered much interest as drug delivery systems since their surface charge, hydrophilicity, and functionality can be purposely modulated.[3,4] Given the diversity of polymeric nanostructures, the therapeutic cargos can be encapsulated in the core, entrapped within the polymer matrix, chemically bound to the polymer, or electrostatically adsorbed on the nanocarrier's surface. These design choices directly influence release kinetics and enable the delivery of hydrophobic and hydrophilic payloads (small-molecule drugs, nucleic acids, and proteins).[5,6]

An accurate characterization of the therapeutic agent release kinetics from the nanocarrier is crucial for optimizing the drug delivery system's safety, efficacy, and clinical performance.[7,8] In the case of protein-loaded nanocarriers, several high-throughput techniques are commonly employed to quantify the released protein, including high-performance liquid chromatography (HPLC) with

[a] *Institut de Ciència de Materials de Barcelona (ICMAB-CSIC), Campus UAB, 08193 Bellaterra, Spain. E-mail: asole@icmab.es, roig@icmab.es*
[b] *Department of Biological Chemistry, Institute for Advanced Chemistry of Catalonia (IQAC-CSIC), 08034 Barcelona, Spain. E-mail: silvia.pujals@iqac.csic.es*
[c] *Dipartimento di Scienze Matematiche, Fisiche e Informatiche, Università di Parma, 43124 Parma, Italy*

UV-visible detection,[9] fluorescence and UV-visible spectroscopy,[7,10–12] enzyme-linked immunosorbent assay (ELISA),[13] and dye-based absorbance methods such as bicinchoninic acid (BCA) and Bradford assays.[14–19] While current techniques effectively quantify the released cargo, a universal standard method is lacking because the optimal technique selection depends on the nanocarrier's composition. More critically, these approaches require sample processing that could alter the nanocarriers, such as centrifugation and filtration, and provide ensemble-averaged information, averaging over millions of particles that masks single-particle heterogeneity. For drug delivery, understanding heterogeneity in loading and release is increasingly recognized as crucial.[20–24] What if we could directly observe individual nanoparticles in action without sample manipulation, tracking payload release at the single-particle level? This study provides a practical, operational method for accessing the missing layer of information.

Over the last decades, the development of super-resolution microscopies has enabled the dissection of cells, subcellular compartments, and even biomolecular assemblies with nanometric resolution.[25–32] While these techniques were first developed for imaging cellular structures, their utility now extends far beyond biology, offering significant benefits to nanotechnology and nanomedicine thanks to current developments in reliable quantification with super-resolution microscopy.[33–37] They contribute to the characterization of nanomaterials and the loaded therapeutics,[38–41] as well as their intracellular trafficking.[42–49] Among the different super-resolution microscopy techniques, stochastic optical reconstruction microscopy (STORM) is a single-molecule localization technique that routinely achieves a lateral resolution of $\sim$20 nm,[25,35,50] and offers the possibility of multi-color imaging and single-molecule sensitivity.[33,51] These features, together with the ability to perform particle-by-particle analysis and the advantage of localizing dye-labelled molecules within the nanoparticle sample, are especially suitable to complement other existing techniques and extend our understanding of cargo release from a nanocarrier. Beyond super-resolution approaches, other microscopy techniques have emerged to investigate nanomaterials in biologically relevant environments, such as soft X-ray microscopy, providing label-free, quantitative imaging of chemically heterogeneous nanostructures with spatial resolutions down to a few nanometers.[52,53] X-ray methods offer a higher penetration depth but lower chemical specificity compared to super-resolution microscopy.

To the best of our knowledge, we present here the first study demonstrating that super-resolution microscopy is a reliable tool for revealing the fine details of cargo release from polymeric nanocarriers at the single-particle level, complementing existing high-throughput methods commonly used in the pharmaceutical industry. For this purpose, we prepared poly(lactic-*co*-glycolic acid) (PLGA) nanocapsules (NCs) fluorescently labelled with Cyanine5 (Cy5) and loaded with fluorescent bovine serum albumin tagged with Alexa Fluor 488 (BSA-AF488), used as a model protein. A thorough characterization using advanced electronic and super-resolution microscopy techniques confirmed the encapsulation of the protein. In this work, we used direct STORM (dSTORM) to visualize the proteins within the PLGA nanocarriers at different time points, followed by an analysis routine implemented in MATLAB, which was employed to automatically extract single-particle data, enabling the study of the evolution of both the nanocarrier and the released fluorescent protein over time. Remarkably, dSTORM results show a similar release profile as when using a Bradford assay, but in addition, evidence the heterogeneity in the protein release between nanocarriers, contributing to a more detailed understanding of drug delivery complexity.

2. Results and discussion

2.1. Nanocarrier characterization

The biocompatible, biodegradable, and FDA-approved polymer PLGA was used to form NCs, with BSA incorporated within their inner cavity as a model for protein delivery.[54] Fluorescent PLGA-Cy5 NCs loaded with fluorescent BSA-AF488 (PLGA-Cy5/BSA-AF488 NCs) were prepared following a double emulsion-solvent evaporation method,[55,56] as described in the SI. Commercial PLGA (acid-terminated) was chemically modified to form PLGA-NH_2, which was linked to Cy5 red dye to obtain PLGA-Cy5, as reported in previous works.[57–60] The final red fluorescent PLGA-Cy5 NCs contained 1% of PLGA-Cy5 and 99% of unlabeled PLGA, while a 20% fraction of the total encapsulated BSA was conjugated with the green AF488 dye and the other 80% was unlabeled BSA. Fig. 1a depicts a scheme of the system. Fig. 1b shows a scanning electron microscopy (SEM) image of the PLGA NCs, evidencing the homogeneity and lack of aggregation. Their spherical morphology and empty core, suitable for accommodating biomolecules, can be seen in Fig. 1c and d, respectively. In cryogenic transmission electron microscopy (cryo-TEM) images of Fig. 1e, the higher electron density of the NC core of protein-loaded PLGA NCs (right) compared to the empty one (left) validates the protein encapsulation inside the nanocarrier. A comparison of the electron intensity profiles is shown in Fig. S1. This was also confirmed by scanning-transmission electron microscopy-energy dispersive X-rays (STEM-EDX), showing a higher nitrogen content (in pink) in the protein-loaded nanocarriers due to the amino acid residues (Fig. 1f). The elemental quantification by STEM-EDX showing the nitrogen band in BSA-loaded NCs can be seen in Fig. S2. PLGA-Cy5/BSA-AF488 NCs had a mean hydrodynamic diameter of 278 $\pm$ 57 nm and a surface charge of –29 $\pm$ 6 mV (Fig. S3).

The fluorophores used to label the nanocarriers (Cy5) and the protein (AF488) were chosen to be spectrally separated for dSTORM imaging. Cy5 and AF488 are standard dyes for dSTORM, widely employed for their excellent photo-switchable properties.[61] Fig. 1g shows a conventional fluorescence image of the nanocarriers compared to the corresponding dSTORM image (Fig. 1h), and the insets show a representative NC for both imaging modes. The increased resolution of dSTORM can resolve individual nanocarriers, allowing an accurate visualization of the protein cargo. In dSTORM, each dot corresponds to one localization, that is, one blinking (on/off switching) event

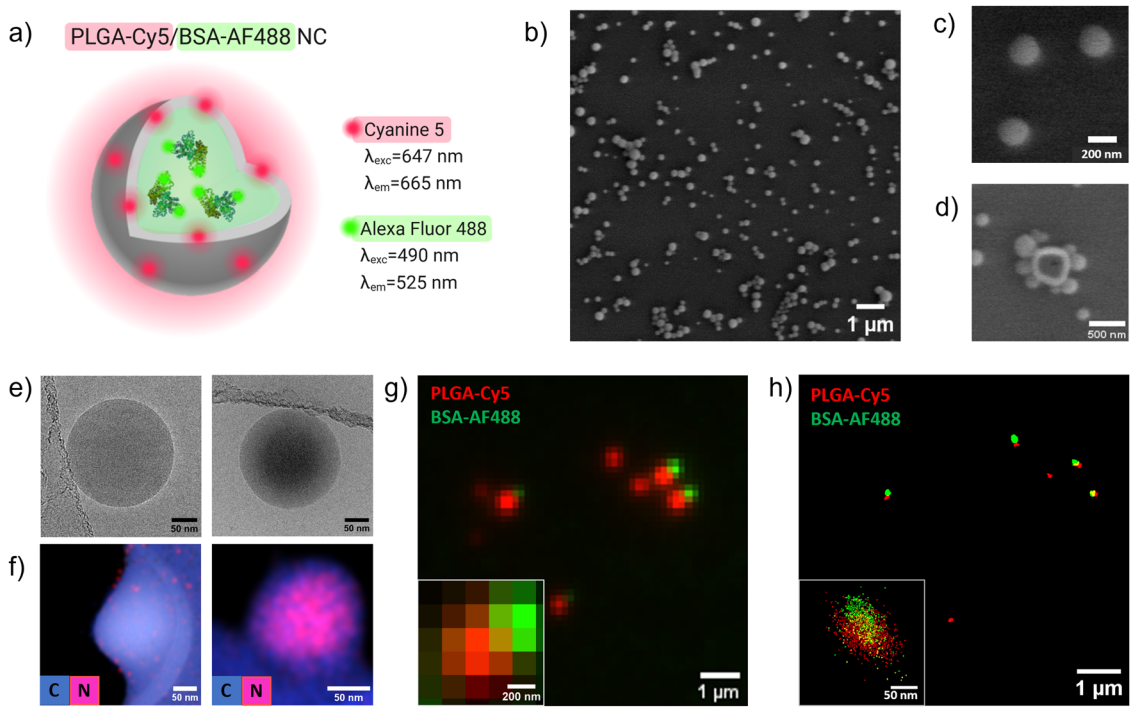

Fig. 1 PLGA nanocarrier design and characterization. (a) Scheme of a PLGA-Cy5/BSA-AF488 NC: PLGA labelled with Cyanine 5 (Cy5) used to encapsulate bovine serum albumin (BSA) labelled with Alexa Fluor 488 (AF488). (b) SEM image of homogeneous PLGA nanocarriers. (c) SEM image showing their spherical morphology. (d) SEM image revealing the hollow core of PLGA nanocarriers formed *via* double emulsion. (e) Cryo-TEM images of an empty (left) and a BSA-loaded (right) PLGA NC. (f) STEM-EDX images of an empty (left) and a BSA-loaded (right) PLGA NC (carbon: blue, nitrogen: pink). (g) Low-resolution image of PLGA NC, with inset showing a single NC. Mechanical drift between sequential channels could not be corrected in the low-resolution imaging mode. (h) Super-resolution image of PLGA NCs, with a Gaussian representation to enhance contrast. The inset shows a single NC with the cross representation.

of a dye, and the image reconstruction is based on single-molecule localization. Using a MATLAB code, we could identify and extract information about the nanocarriers' size and study the cargo release from the NCs.

2.2. STORM data analysis workflow

Following dSTORM imaging, the position and time coordinates of three different channels were extracted: nanocarriers (647), proteins (488), and fiducial markers used for drift correction (561). These data were then analyzed with a refined MATLAB code, schematically shown in Fig. 2, in which the implemented upgrades to the original code from ref. 62 are represented in yellow. Firstly, the centers of the nanocarriers and fiducial markers were identified using a mean-shift clustering algorithm, which works by grouping nearby points based on their density. Once the centers were located, the nanocarrier channel was filtered by different criteria: number of localizations, nanocarrier diameter, distance between nanocarrier centers, elongation, and proximity to fiducial markers (detailed explanation in the SI). After filtering, the program estimated the center and diameter of each nanocarrier based on the positions of its localizations. Given the automatic detection and quantification of the dye localizations, many NCs could be identified in each image, providing a particle-by-particle distribution of their diameter and localizations.

Finally, the non-released protein localizations during the release experiment were defined relative to each individual nanocarrier by introducing a size-dependent proximity criterion. Protein localizations were considered associated with a given NC if they were located within a circular region centered at the NC, with radius equal to the NC radius multiplied by a scaling factor, set to 1.3. This included proteins still inside the nanocarrier (colocalized with PLGA-Cy5) or near to its edge (within 30% safety margin). This margin, absent in the original analysis code, accounts for time-dependent size changes caused by polymeric degradation over time. The value of this scaling factor was determined through optimization to ensure that we captured truly associated proteins, minimizing false positives from distant proteins, and to account for the limited localization precision of dSTORM, including protein molecules that appeared slightly outside the boundary due to single-molecule localization uncertainty. Knowing the protein localizations still bound to the nanocarriers, we could extract the fraction of protein released at each time point.

Detailed parameter optimization can be found in the SI. All codes required to perform the full analysis are available in a GitHub repository,[63] along with detailed information on their functioning and example files for testing and running the workflow.

Having established the robustness of this analysis, we first studied the time evolution of the PLGA nanocarriers by

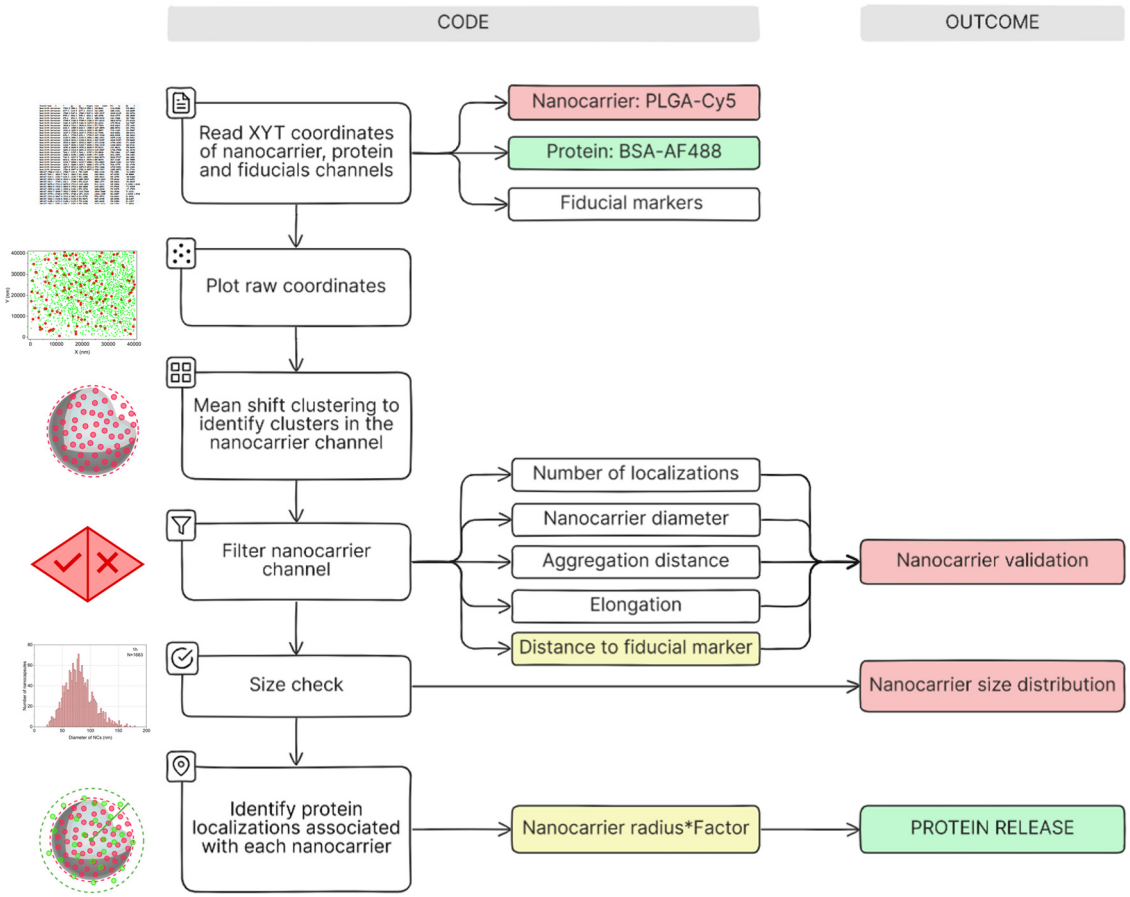

Fig. 2 MATLAB code diagram and nanocarrier information outcomes. The flowchart illustrates the sequential steps the code follows. The upgrades to the original code developed in ref. 62 are highlighted in yellow and were implemented to adapt to the PLGA nanocarrier evolution during protein release. Red entries correspond to outcomes associated with the nanocarriers' (PLGA-Cy5) characteristics, while green entries refer to the protein release with time (BSA-AF488). Diagram created with Eraser.

dSTORM, determining their size and PLGA degradation and complementing these analyses with other particle analysis techniques. Next, we assessed the time-dependent release of the protein from the nanocarriers.

2.3. Nanocarrier time evolution

We then used dSTORM imaging and the previously described analysis methodology to investigate the time-dependent morphological changes of the nanocarriers. PLGA-Cy5/BSA-AF488 NCs were incubated in PBS 1X (pH = 7.4) at a concentration of 5 mg mL^{-1} of NCs at 37 °C, and sampled at different time points (0 h, 1 h, 12 h, 1 day, 4 days, 16 days, and 30 days).

Fig. 3a shows the time evolution of the mean nanocarrier diameter measured by dSTORM (in red). A significant increase in diameter over time is observed, especially after 4 days, as shown in the nanoparticle tracking analysis (NTA) data (grey in Fig. 3a). These size variations over time are likely due to a combination of processes, including PLGA hydration and swelling of the NCs, bulk hydrolysis, PLGA fragment fusion, and aggregation.[64–66]

The descriptive statistics and size distributions obtained by dSTORM and NTA are displayed in Table S1 and Fig. S4. The apparent discrepancy between dSTORM and NTA particle sizes (70–110 nm *vs.* 230–330 nm, respectively) arises from fundamental differences in the measurements each technique makes. NTA reports the hydrodynamic diameter, which includes the particle core and the surrounding electrical double layer of solvent molecules that move with the particle.[67] In contrast, dSTORM provides a measurement closer to the fluorescently labelled nanocarrier, which is smaller than the hydrodynamic diameter. Importantly, Cy5 distribution can lead to dSTORM underestimating size. Since localization algorithms discard blinking events below a specific threshold, this may partially shrink the apparent radius toward the region of highest fluorophore density and best signal-to-noise ratio.[68] Additionally, NTA assumes a spherical diffusion model, which is generally appropriate. Still, aggregates or debris can lead to deviations from sphericity, resulting in non-spherical particles being detected as larger apparent spheres. This effect can contribute to an overestimation of particle size by NTA. Conversely, dSTORM enables straightforward identification and exclusion of such aggregates, a capability that is more limited in NTA measurements.

NTA further revealed a significant decrease in the number of NCs, especially important after 4 days (Fig. 3b). A schematic

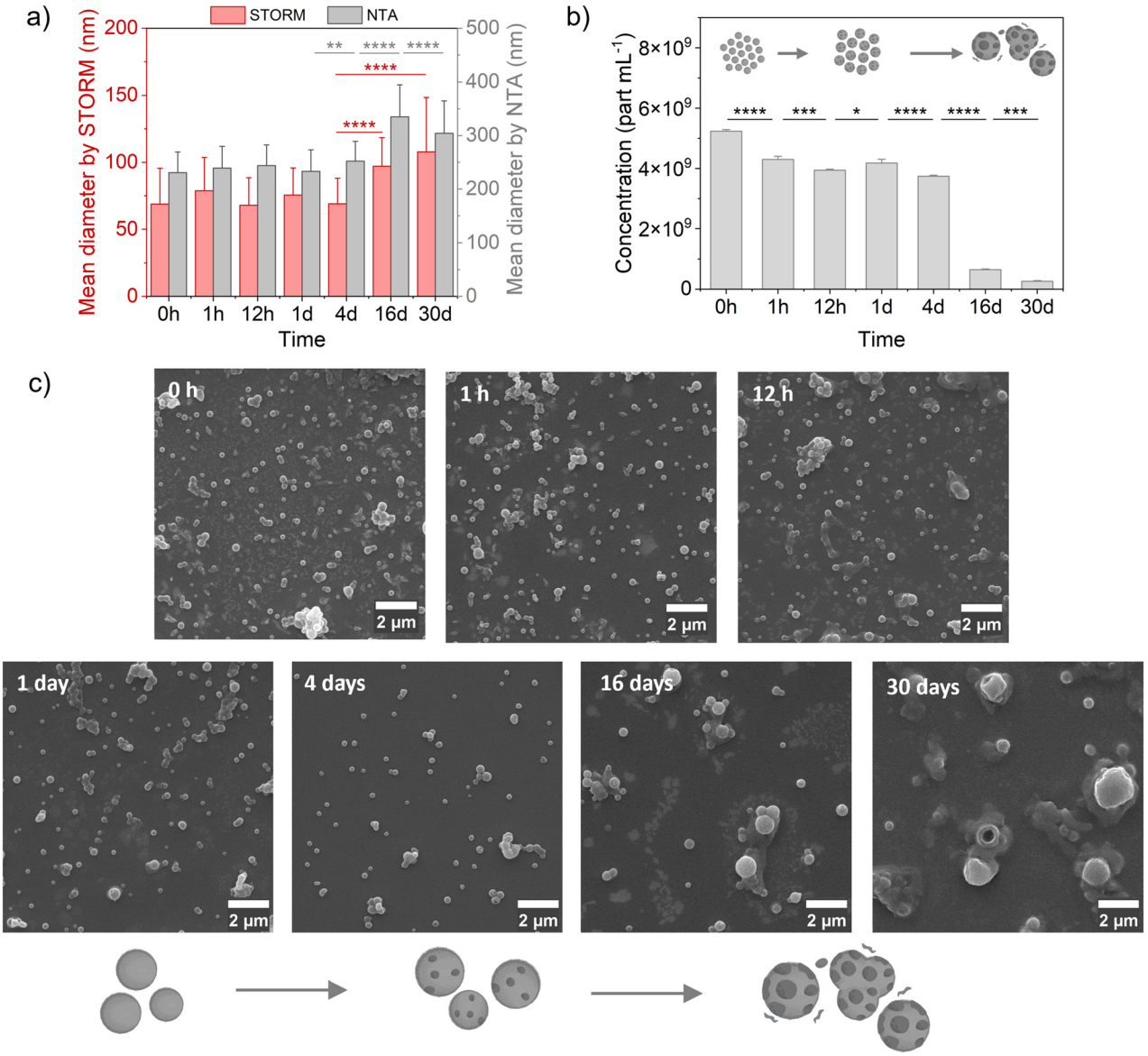

Fig. 3 Nanocarrier monitoring at different time points by dSTORM, NTA and SEM. (a) Mean diameter ± standard deviation (SD) in nm given by dSTORM (red) and NTA (grey). Sample size for dSTORM data: N = 594 (0 h), N = 1663 (1 h), N = 1712 (N = 12 h), N = 2843 (1 day), N = 525 (4 days), N = 236 (16 days), N = 30 (30 days). P-Values are calculated using one-way ANOVA with Tukey's multiple comparison test (**$P < 0.01$, and ****$P < 0.0001$). Statistical tests were run separately for dSTORM and NTA. Error bars of NTA data correspond to the SD of the size distribution, not the SD between the three replicates. (b) NCs concentration ± SD (particles mL^{-1}) given by NTA. P-Values are calculated using one-way ANOVA with Tukey's multiple comparison test (*$P < 0.05$, **$P < 0.01$, ***$P < 0.001$, and ****$P < 0.0001$). The schematic drawing shows the decrease of NC concentration. (c) SEM images of the NCs at different time points, where nanocarrier degradation is visible at extended periods (16 and 30 days). The schematic representation depicts the morphological evolution of nanocarriers due to multiple processes (polymer hydration, swelling, hydrolytic degradation followed by fusion of PLGA fragments, and a certain degree of aggregation).

illustration is included in the same panel to visually represent the drop in nanocarrier concentration. This suggests that hydrolytic degradation of PLGA is occurring, evidencing the dynamic and complex nature of the system, which must be considered in the release studies. The number of Cy5 localizations per NC could also be assessed by dSTORM (Fig. S5), which showed a clear decrease at 30 days, substantiating PLGA-Cy5 degradation, therefore not adhering to the surface of the glass slide.

SEM confirmed the morphological changes and hydrolysis effects on the nanocarriers (Fig. 3c). In the same figure, a schematic representation of the proposed morphological evolution is shown. At early time points, the nanocarriers appeared spherical and of very similar size, with some small aggregates likely caused by NCs collapse after water evaporation during sample preparation. By days 16 and 30, larger spherical structures were evident, which could reflect the combined effects of the above-mentioned processes.

2.4. Protein release

dSTORM was then used to quantitatively monitor the release of cargo from the nanocarrier at the single-particle level. Representative dSTORM images of individual nanocarriers are shown in Fig. 4a, where the nanocarrier (PLGA-Cy5) localizations appear in red and the localizations of the protein (BSA-AF488) associated with the nanocarrier (unreleased protein) in green. The different images do not correspond to the same particle, as the release experiment was performed in a vial and aliquots were taken for imaging at given time points. The nanocarrier size, determined from the analysis of the PLGA-Cy5 localizations, is shown with the red circle, containing the 95% of the datapoints. BSA-AF488 localizations close to the nanocarrier, within the green circle (1.3 times the radius of each nanocarrier), are considered unreleased. In contrast, released BSA-AF488 localizations located further away from the nanocarrier, outside the green circle, are shown in white. Note that the number of encapsulated proteins decreased over time, and nanocarrier degradation was clearly evidenced at 30 days by the very few Cy5 detected localizations, suggesting that nearly all NCs have degraded.

After MATLAB-based data analysis, the number of unreleased protein localizations per nanocarrier at each time point were obtained. Histograms of protein localizations per nanocarrier are shown in Fig. S6. Notably, the single-molecule sensitivity of dSTORM revealed significant heterogeneity between nanocarriers, showing that, for a given time point, some particles had a considerable amount of encapsulated protein and others had much less. This heterogeneity was quantified through distribution fitting. The box plots are shown in Fig. S7, and the statistical magnitudes are collected in Table S2, with a large

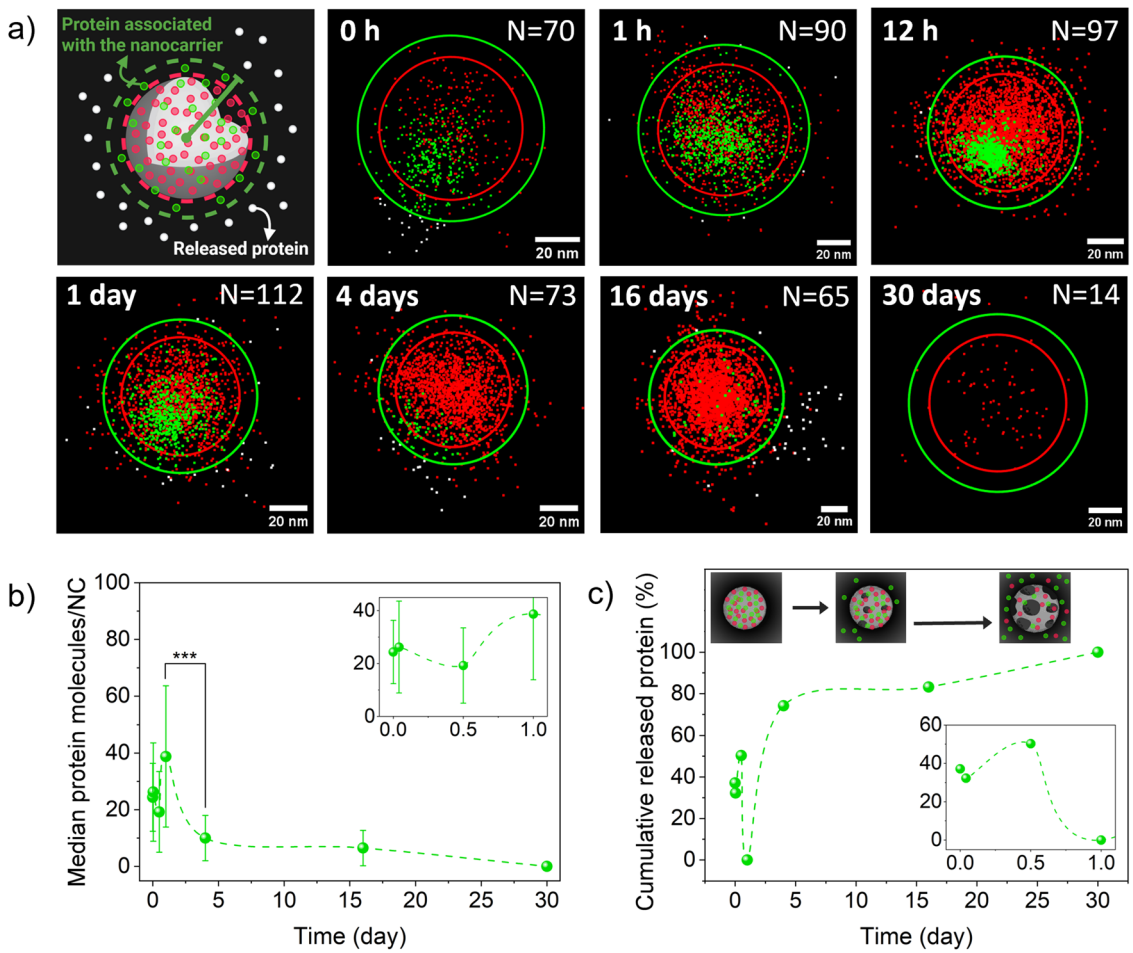

Fig. 4 Protein release from PLGA NCs by dSTORM. (a) dSTORM images of an individual NC representative of each time point. In the rendering of dSTORM images, localizations are shown with the cross representation to better discriminate the red and green localizations. Red dots: PLGA-Cy5 localizations; green dots: BSA-AF488 localizations associated with the NC; white dots: released BSA-AF488 localizations; red circle: nanocarrier size (containing 95% of Cy5 localizations); green circle: circle that contains the BSA-AF488 localizations associated with the NC (radius of each nanocarrier multiplied by a scaling factor). The number of nanocarriers analyzed at each time is indicated: N = 70 (0 h), N = 90 (1 h), N = 97 (N = 12 h), N = 112 (1 day), N = 73 (4 days), N = 65 (16 days), N = 14 (30 days). (b) Median protein molecules per NC *vs.* time. Error bars show the median absolute deviation (MAD). P-Values are calculated using Kruskal–Wallis test with Dunn's multiple comparison test (***$P < 0.001$). Inset shows the data points during the first day. (c) Cumulative percentage of median released protein *vs.* time. The inset graph shows the data points from the first day. Error bars are not shown for graph clarity. The illustration schematically depicts the hydrolysis process that triggers the release. Dashed green lines in (b) and (c) are included as a guide to the eye.

interquartile range (IQR), evidencing the variability between nanocarriers. These results complement the nanoscale heterogeneity already reported in other studies employing super-resolution microscopy, including investigations of nanoparticle surface functionalization,[69] protein corona formation,[70–72] extracellular vesicles secretion,[73] homogeneous supramolecular polymers,[74] and single-crystal nanocomposites,[75] going beyond ensemble-averaged techniques.

To convert these localization counts into an estimate of the number of protein molecules per nanocarrier, a calibration based on single proteins was performed (detailed protocol in SI and results in Fig. S8). Specifically, the number of localizations generated by individual labeled proteins was determined and used to estimate the number of proteins associated with each PLGA NC, following previously reported approaches.[70,76–78] To improve the accuracy of the estimation, a single-molecule blinking calibration was performed under the same imaging conditions as the release experiment, thereby minimizing potential errors arising from differences in the chemical environment.

The median number of unreleased protein molecules per nanocarrier decreased with time after 1 day (Fig. 4b), indicating their release from the NCs. The apparent decreased protein molecules at the earliest time points may be due to the limited penetration of the STORM imaging buffer into the nanocarriers, which could impair AF488 switching and lead to an underestimation of detected localizations. After longer incubation (*e.g.*, 24 h at 37 °C), partial hydrolysis of the PLGA matrix may increase particle porosity, potentially facilitating buffer penetration and improving detection efficiency.

It is important to note that it was not possible to unambiguously distinguish between nanocarriers that were initially empty and those that became empty due to complete release. Therefore, our analysis focused on the temporal evolution of the distribution of protein molecules per nanocarrier, rather than on the absolute identification of empty particles.

Additionally, the fraction of released protein was calculated following eqn (1). Since the highest number of detected protein molecules per nanocarrier occurred at t = 1 day, this value was used as a reference maximum, corresponding to the maximum detectable number of protein per nanocarrier. The median number of protein molecules/NC at time t was subtracted from this maximum value and normalized accordingly to obtain the fractional release. As seen in Fig. 4c, a rapid release (burst) occurred over the first 4 days, followed by a sustained regime, reaching complete release after 30 days, in which PLGA degradation is evident. This biphasic release profile was also obtained using the Bradford assay (Fig. S9), which provided averaged protein quantification and aligned with the results shown in other studies.[79–82]

$$\%\,\text{Released protein} = \frac{\text{maximum protein} - \text{unreleased protein}}{\text{maximum protein}} \quad (1)$$

Both fluorophores (Cy5, covalently linked to PLGA, and AF488, coupled to BSA) exhibited high photophysical stability over time, with negligible spectral shifts and minimal intensity variation (Fig. S10). This rules out any miscounting of protein localizations due to dye degradation.

Although STORM can be considered a low-throughput technique due to the time required for imaging and data processing, it allowed direct observation of nanocarrier size and cargo localization simultaneously with spatial resolution far surpassing bulk techniques such as NTA. In contrast, NTA is a high-throughput technique that provides population-level statistics on the size, number, and diffusion of nanocarriers, but it does not allow for the study of cargo release. Furthermore, while protein quantification by bulk techniques such as Bradford or BCA assays offers rapid, quantitative, and averaged release profiles across the entire nanoparticle population, dSTORM has the potential to reveal subparticle spatial patterns with minimal sample manipulation, enabling the direct observation of cargo release or protein corona formation, processes that bulk methods cannot capture with such detail. Our particle-by-particle analysis ensured that only protein localized within the nanocarriers was quantified, excluding any unencapsulated protein present in suspension, an assessment not attainable with ensemble approaches. dSTORM also allows multicolor imaging, enabling the simultaneous tracking of nanocarriers along with multiple cargoes, a valuable feature for studying the loading and release of a combination of drugs. In addition, conventional protein quantification methods require concentrations above their detection limit (typically in the μg mL^{-1} range). Conversely, dSTORM's high sensitivity enables the detection of single-molecule events, making it particularly advantageous when protein levels are extremely low.

3. Conclusions

This study proposes dSTORM as an emerging tool for the visualization and quantification of proteins released from polymeric nanocarriers at the single-particle level with nanometric accuracy, integrating other advanced microscopy techniques, such as cryo-TEM and STEM-EDX. Remarkably, this represents the first-ever application of super-resolution microscopy to monitor cargo release from any nanocarrier. dSTORM generates vast data sets of dye localizations, requiring specialized software for efficient analysis. To address this, we modified a previously developed MATLAB code to account for the temporal evolution resulting from the hydrolytic degradation of PLGA nanocarriers. This updated code is now publicly available in an online open repository. Our analysis revealed an increase in NCs diameter over time, likely attributable to hydration, swelling and hydrolytic degradation, followed by fusion of partially degraded PLGA fragments, further corroborated by NTA. SEM images showed well-dispersed and homogeneous nanocarriers at the initial time points, whereas morphological changes were evident at 16 and 30 days. Additionally, the concentration of nanocarriers decreased over time, confirming their degradation.

Thus, the most challenging part of this work was studying the release of BSA-AF488 from the dynamically transforming PLGA NCs. The particle-by-particle analysis revealed a rapid

release of the protein up to 4 days, followed by a sustained regime, achieving complete protein release within 30 days. Remarkably, the heterogeneity between NCs was only discernible due to the single-molecule sensitivity of dSTORM, giving a realistic picture of the system at the single-particle level and surpassing ensemble-averaged information. Furthermore, dSTORM imaging enabled the simultaneous observation of nanocarrier degradation and cargo release, while conventional ensemble techniques typically allow monitoring of only one of these processes at a time.

Our work provides a foundation for further studies since it demonstrated the feasibility to study protein release in complex nanocarrier systems by super-resolution microscopy. Having established this protocol and adaptable data treatment software, dSTORM now has the potential to be applied to other polymeric drug delivery systems (*i.e.*, PLGA-PEG, lipid-polymer hybrids), other cargo types (*i.e.*, therapeutic proteins, antibodies, nucleic acids), and to multi-cargo release (*via* multicolor STORM) to validate this methodology. Some limitations of this approach include the need for fluorescent labeling of both carrier and cargo, a potential photobleaching bias, and the constraint of not being a high-throughput approach.

Conflicts of interest

The authors declare no conflicts of interest.

Data availability

All data supporting the findings in this paper are included in the main text and supplementary information (SI). Supplementary information includes the materials and methods details, including the synthesis of PLGA-Cy5/BSA-AF488 NCs, the sample preparation for characterization (cryo-TEM, STEM-EDX, SEM, and NTA), *in vitro* release experiment, dSTORM sample preparation, imaging, and data analysis, validation of analysis parameters for nanocarrier identification and protein release quantification, calibration of AF488 localizations per protein molecule, fluorophore stability assessment, and statistical analysis. The supplementary figures show cryo-TEM images analysis, elemental EDX quantification, size distribution and Z-potential by DLS, size distribution by dSTORM and NTA, histograms of PLGA-Cy5 localizations by dSTORM, histograms and box plots of BSA-AF488 localizations per NC by dSTORM, histogram and box plot of the number of AF488 localizations per protein molecule (calibration), comparison of protein release quantification by dSTORM and Bradford assay, fluorophore stability over time (Cy5 and AF488), control dSTORM images to discard cross-channel blinking, discarded NCs, box plots of protein localizations per NC using different scaling factors. See DOI: https://doi.org/10.1039/d5nh00855g.

Acknowledgements

The authors acknowledge the CEX2023001263-S (''Severo Ochoa'' Program for Center of Excellence in R&D), funded by MCIN/AEI/10.13039/501100011033 and by FEDER, ''A way of making Europe'', as well as La Marató TV3 (202333-30 grant). S. Pujals is grateful for CNS2023-145136 (''Consolidación Investigadora 2023'') and Retos I + D + i national project PID2024-162181OB-I00 funded by AEI. A. Solé-Porta acknowledges the PhD scholarship (FPU21/04142) in the framework of the Materials Science PhD program of the Universitat Autònoma de Barcelona. The authors acknowledge M. Milozzi and G. Romero from IBEC Microscopy Characterization facility for the support during dSTORM data acquisition. The authors thank Dr P. Guerra from the IBMB-CSIC CryoEM Platform for assistance during microscope data acquisition (Project IU16-014045 CRYO-TEM, Generalitat de Catalunya). The authors also acknowledge Dr B. Mundet and K. Gupta for support during STEM imaging, as well as the use of instrumentation financed through grant IU16-014206 (METCAM-FIB) funded by the European Union through the European Regional Development Fund (ERDF), with the support of the Ministry of Research and Universities and Generalitat de Catalunya. The authors thank Dr J. Oró from ICMAB for STEM sample preparation and analysis and J. A. Bernabé and Unit 6 of the ICTS ''NANBIOSIS'' for the NTA measurements. Figures were created using https://Biorender.com.

References

1 M. J. Mitchell, M. M. Billingsley, R. M. Haley, M. E. Wechsler, N. A. Peppas and R. Langer, *Nat. Rev. Drug Discovery*, 2020, **20**, 101–124.
2 J. K. Patra, G. Das, L. F. Fraceto, E. V. R. Campos, M. D. P. Rodriguez-Torres, L. S. Acosta-Torres, L. A. Diaz-Torres, R. Grillo, M. K. Swamy, S. Sharma, S. Habtemariam and H. S. Shin, *J. Nanobiotechnol.*, 2018, **16**, 1–33.
3 A. Chan and A. Tsourkas, *BME Front.*, 2024, **5**, 0035.
4 H. Zhao, Z. Y. Lin, L. Yildirimer, A. Dhinakar, X. Zhao and J. Wu, *J. Mater. Chem. B*, 2016, **4**, 4060–4071.
5 M. MacHtakova, H. Thérien-Aubin and K. Landfester, *Chem. Soc. Rev.*, 2022, **51**, 128–152.
6 A. Vardaxi, M. Kafetzi and S. Pispas, *Polymers*, 2022, **14**, 777.
7 J. Smith, K. G. Sprenger, R. Liao, A. Joseph, E. Nance and J. Pfaendtner, *Biointerphases*, 2017, **12**, 2–412.
8 S. R. Falsafi, H. Rostamabadi, E. Assadpour and S. M. Jafari, *Adv. Colloid Interface Sci.*, 2020, **280**, 102166.
9 S. Vanni, T. M. Caputo, A. M. Cusano, A. De Vita, A. Cusano, C. Cocchi, C. Mulè, S. Principe, C. Liverani, G. Celetti, A. Micco, C. Spadazzi, G. Miserocchi, T. Ibrahim, L. Mercatali and A. Aliberti, *Nanoscale*, 2025, **17**, 9436–9457.
10 F. Wang, Y. Deng, J. Wang, L. Yu, F. Ding, W. Lian, Q. Liu and X. Lin, *Drug Delivery*, 2021, **28**, 865–872.
11 C. E. Markwalter, R. F. Pagels, A. N. Hejazi, K. D. Ristroph, J. Wang, K. Chen, J. Li and R. K. Prud'homme, *J. Controlled Release*, 2021, **334**, 11–20.
12 S. Akpinar Adscheid, M. Rojas-Rodríguez, S. M. Abdel-Hafez, F. S. Pavone, M. Schneider, A. E. Türeli, M. Calamai and N. Günday-Türeli, *Pharmaceutics*, 2025, **17**, 87.
13 H. Wang, Y. Gao, J. Wang, M. Cao, G. Dai, P. Lu, R. Sheng, C. Zhang, Q. Wang, G. Li, Q. Y. H. Ai, Y. Rui and L. Shi, *ACS Nano*, 2025, **19**, 13871–13888.

14 M. Clerici, L. C. Nelemans, M. Buzgo and A. Simaite, *Proceedings*, 2020, **78**, 28.
15 J. Wu, N. Kamaly, J. Shi, L. Zhao, Z. Xiao, G. Hollett, R. John, S. Ray, X. Xu, X. Zhang, P. W. Kantoff and O. C. Farokhzad, *Angew. Chem., Int. Ed.*, 2014, **53**, 8975.
16 X. Chen, S. S. Moonshi, N. T. Nguyen and H. T. Ta, *Nanotechnology*, 2023, **35**, 055101.
17 M. Jin, S. H. Seo, B. S. Kim, S. Hwang, Y. G. Kang, J. W. Shin, K. H. Cho, J. Byeon, M. C. Shin, D. Kim, C. Yoon and K. A. Min, *Pharm. Res.*, 2021, **38**, 1455–1466.
18 R. Rietscher, J. A. Czaplewska, T. C. Majdanski, M. Gottschaldt, U. S. Schubert, M. Schneider and C. M. Lehr, *Int. J. Pharm.*, 2016, **500**, 187–195.
19 S. Vakilian, S. Mashayekhan, I. Shabani, M. Khorashadizadeh, A. Fallah and M. Soleimani, *Int. J. Biol. Macromol.*, 2015, **75**, 248–257.
20 J. Morla-Folch, A. Ranzenigo, Z. A. Fayad and A. J. P. Teunissen, *Small*, 2024, **20**, 2307502.
21 C. Saunders, J. E. J. Foote, J. P. Wojciechowski, A. Cammack, S. V. Pedersen, J. J. Doutch, H. M. G. Barriga, M. N. Holme, J. Penders, M. Chami, A. Najer and M. M. Stevens, *ACS Nano*, 2023, **17**, 11713–11728.
22 C. W. Beh, D. Pan, J. Lee, X. Jiang, K. J. Liu, H. Q. Mao and T. H. Wang, *Nano Lett.*, 2014, **14**, 4729–4735.
23 C. Chen, S. Zhu, S. Wang, W. Zhang, Y. Cheng and X. Yan, *ACS Appl. Mater. Interfaces*, 2017, **9**, 13913–13919.
24 S. Li, Y. Hu, A. Li, J. Lin, K. Hsieh, Z. Schneiderman, P. Zhang, Y. Zhu, C. Qiu, E. Kokkoli, T. H. Wang and H. Q. Mao, *Nat. Commun.*, 2022, **13**, 5561.
25 S. J. Sahl, S. W. Hell and S. Jakobs, *Nat. Rev. Mol. Cell Biol.*, 2017, **18**, 685–701.
26 L. Schermelleh, A. Ferrand, T. Huser, C. Eggeling, M. Sauer, O. Biehlmaier and G. P. C. Drummen, *Nat. Cell Biol.*, 2019, **21**, 72–84.
27 M. Sauer and M. Heilemann, *Chem. Rev.*, 2017, **117**, 7478–7509.
28 N. Sun, Y. Jia, S. Bai, Q. Li, L. Dai and J. Li, *Adv. Colloid Interface Sci.*, 2023, **314**, 102880.
29 L. A. Masullo, R. Kowalewski, M. Honsa, L. Heinze, S. Xu, P. R. Steen, H. Grabmayr, I. Pachmayr, S. C. M. Reinhardt, A. Perovic, J. Kwon, E. P. Oxley, R. A. Dickins, M. M. C. Bastings, I. A. Parish and R. Jungmann, *Nat. Commun.*, 2025, **16**, 1–11.
30 E. Betzig, G. H. Patterson, R. Sougrat, O. W. Lindwasser, S. Olenych, J. S. Bonifacino, M. W. Davidson, J. Lippincott-Schwartz and H. F. Hess, *Science*, 2006, **313**, 1642–1645.
31 Y. M. Sigal, R. Zhou and X. Zhuang, *Science*, 2018, **361**, 880–887.
32 M. Honsa, I. Pachmayr, L. Heinze, L. Bas, L. A. Masullo, J. Kwon, A. Perovic, B. Schulman and R. Jungmann, *Small Methods*, 2025, 2401799.
33 S. Pujals and L. Albertazzi, *ACS Nano*, 2019, **13**, 9707–9712.
34 D. Wöll and C. Flors, *Small Methods*, 2017, **1**, 1700191.
35 S. Pujals, N. Feiner-Gracia, P. Delcanale, I. Voets and L. Albertazzi, *Nat. Rev. Chem.*, 2019, **3**, 68–84.
36 S. Dhiman, T. Andrian, B. S. Gonzalez, M. M. E. Tholen, Y. Wang and L. Albertazzi, *Chem. Sci.*, 2022, **13**, 2152–2166.
37 S. Hugelier, P. L. Colosi and M. Lakadamyali, *Annu. Rev. Biophys.*, 2023, **52**, 139–160.
38 N. Feiner-Gracia, R. A. Olea, R. Fitzner, N. El Boujnouni, A. H. Van Asbeck, R. Brock and L. Albertazzi, *Nano Lett.*, 2019, **19**, 2784–2792.
39 X. Shaulli, A. Maria Moreno-Echeverri, M. Andoni, E. Waeber, S. N. Ramakrishna, C. Fritsch, D. Vanhecke, B. Rothen-Rutishauser and F. Scheffold, *Small*, 2025, **21**, 2405929.
40 P. Das, S. Pujals, L. M. A. Ali, M. Gary-Bobo, L. Albertazzi and J. O. Durand, *Nanoscale*, 2023, **15**, 12008–12024.
41 J. I. Gallea, O. Nevskyi, Z. Kaźmierczak, I. Gligonov, T. Chen, P. Miernikiewicz, A. M. Chizhik, L. Reinkensmeier, K. Dąbrowska, M. Bates and J. Enderlein, *Adv. Mater.*, 2025, **37**, 2403365.
42 R. Riera, J. Tauler, N. Feiner-Gracia, S. Borrós, C. Fornaguera and L. Albertazzi, *ChemMedChem*, 2022, **17**, e202100633.
43 V. Sheth, X. Chen, E. M. Mettenbrink, W. Yang, M. A. Jones, O. M'Saad, A. G. Thomas, R. S. Newport, E. Francek, L. Wang, A. N. Frickenstein, N. D. Donahue, A. Holden, N. F. Mjema, D. E. Green, P. L. DeAngelis, J. Bewersdorf and S. Wilhelm, *ACS Nano*, 2023, **17**, 8376–8392.
44 E. J. Guggenheim, A. Khan, J. Pike, L. Chang, I. Lynch and J. Z. Rappoport, *PLoS One*, 2016, **11**, e0159980.
45 H. D. W. Herath and Y. S. Hu, *Nanoscale*, 2025, **17**, 1213–1224.
46 M. Wojnilowicz, A. Glab, A. Bertucci, F. Caruso and F. Cavalieri, *ACS Nano*, 2019, **13**, 187–202.
47 S. K. Bhangu, L. Mummolo, S. Fernandes, A. Amodio, A. Radziwon, B. Dyett, M. Savioli, N. Mantri, C. Cortez-Jugo, F. Caruso and F. Cavalieri, *Adv. Funct. Mater.*, 2024, **34**, 2311240.
48 M. Ojansivu, H. M. G. Barriga, M. N. Holme, S. Morf, J. J. Doutch, S. E. L. Andaloussi, T. Kjellman, M. Johnsson, J. Barauskas and M. M. Stevens, *Adv. Mater.*, 2025, **37**, 2419538.
49 D. Van Der Zwaag, N. Vanparijs, S. Wijnands, R. De Rycke, B. G. De Geest and L. Albertazzi, *ACS Appl. Mater. Interfaces*, 2016, **8**, 6391–6399.
50 S. Van De Linde, A. Löschberger, T. Klein, M. Heidbreder, S. Wolter, M. Heilemann and M. Sauer, *Nat. Protoc.*, 2011, **6**, 991–1009.
51 M. J. Rust, M. Bates and X. Zhuang, *Nat. Methods*, 2006, **3**, 793–795.
52 D. A. Shapiro, S. Babin, R. S. Celestre, W. Chao, R. P. Conley, P. Denes, B. Enders, P. Enfedaque, S. James, J. M. Joseph, H. Krishnan, S. Marchesini, K. Muriki, K. Nowrouzi, S. R. Oh, H. Padmore, T. Warwick, L. Yang, V. V. Yashchuk, Y. S. Yu and J. Zhao, *Sci. Adv.*, 2020, **6**, 4904.
53 K. G. Y. Arsana, G. M. Saladino, B. Brodin, M. S. Toprak and H. M. Hertz, *Int. J. Mol. Sci.*, 2024, **25**, 920.
54 A. Solé-Porta, A. Areny-Balagueró, M. Camprubí-Rimblas, E. Fernández Fernández, A. O'Sullivan, R. Giannoccari, R. MacLoughlin, D. Closa, A. Artigas and A. Roig, *Small Sci.*, 2024, **4**, 2400066.
55 Y. Zhang, M. García-Gabilondo, A. Rosell and A. Roig, *Pharmaceutics*, 2019, **12**, 16.
56 A. Grayston, Y. Zhang, M. Garcia-Gabilondo, M. Arrúe, A. Martin, P. Kopcansky, M. Timko, J. Kovac, O. Strbak, L. Castellote, S. Belloli, R. M. Moresco, M. Picchio, A. Roig and A. Rosell, *J. Cereb. Blood Flow Metab.*, 2022, **42**, 237–252.

57 Y. Zhang, M. García-Gabilondo, A. Grayston, I. V. J. Feiner, I. Anton-Sales, R. A. Loiola, J. Llop, P. Ramos-Cabrer, I. Barba, D. Garcia-Dorado, F. Gosselet, A. Rosell and A. Roig, *Nanoscale*, 2020, **12**, 4988–5002.
58 A. Areny-Balagueró, W. Mekseriwattana, M. Camprubí-Rimblas, A. Stephany, A. Roldan, A. Solé-Porta, A. Artigas, D. Closa and A. Roig, *Pharmaceutics*, 2022, **14**, 1447.
59 S. Sathiensathaporn, A. Solé-Porta, D. Baowan, D. Pissuwan, P. Wongtrakoongate, A. Roig and K. P. Katewongsa, *J. Food Sci.*, 2025, **90**, e17631.
60 A. Grayston, M. Garcia-Gabilondo, N. Otero-Fornés, A. Solé-Porta, I. de la Torre-Sánchez, W. Mekseriwattana, M. Timko, J. Kovac, P. Kopcansky, J. Li, R. Tiberi, M. Esteves, A. Tomasello, D. Hernández, M. Ribó, A. Roig and A. Rosell, *Nanoscale*, 2026, **18**, 3669–3681.
61 G. T. Dempsey, J. C. Vaughan, K. H. Chen, M. Bates and X. Zhuang, *Nat. Methods*, 2011, **8**, 1027–1040.
62 P. Delcanale and L. Albertazzi, *Data Br.*, 2020, **30**, 105468.
63 A. Solé-Porta, S. Pujals, P. Delcanale and A. Roig, *STORM release analysis*, https://github.com/annasoleporta/STORM_release_analysis.
64 H. K. Makadia and S. J. Siegel, *Polymers*, 2011, **3**, 1377–1397.
65 H. Keles, A. Naylor, F. Clegg and C. Sammon, *Polym. Degrad. Stab.*, 2015, **119**, 228–241.
66 D. Hofmann, M. Entrialgo-Castaño, K. Kratz and A. Lendlein, *Adv. Mater.*, 2009, **21**, 3237–3245.
67 C. M. Maguire, M. Rösslein, P. Wick and A. Prina-Mello, *Sci. Technol. Adv. Mater.*, 2018, **19**, 732–745.
68 M. Lelek, M. T. Gyparaki, G. Beliu, F. Schueder, J. Griffié, S. Manley, R. Jungmann, M. Sauer, M. Lakadamyali and C. Zimmer, *Nat. Rev. Methods Prim.*, 2021, **1**, 1–27.
69 R. A. J. Post, D. van der Zwaag, G. Bet, S. P. W. Wijnands, L. Albertazzi, E. W. Meijer and R. W. van der Hofstad, *Nat. Commun.*, 2019, **10**, 1663.
70 N. Feiner-Gracia, M. Beck, S. Pujals, S. Tosi, T. Mandal, C. Buske, M. Linden and L. Albertazzi, *Small*, 2017, **13**, 1701631.
71 T. Patiño, J. Llacer-Wintle, S. Pujals, L. Albertazzi and S. Sánchez, *Nanoscale*, 2024, **16**, 2904–2912.
72 Y. Wang, P. E. D. Soto Rodriguez, L. Woythe, S. Sánchez, J. Samitier, P. Zijlstra and L. Albertazzi, *ACS Appl. Mater. Interfaces*, 2022, **14**, 37345–37355.
73 S. Dechantsreiter, A. R. Ambrose, J. D. Worboys, J. M. E. Lim, S. Liu, R. Shah, M. A. Montero, A. M. Quinn, T. Hussell, G. M. Tannahill and D. M. Davis, *J. Extracell. Vesicles*, 2022, **11**, e12215.
74 E. Archontakis, S. Dhiman, M. Zhang, M. E. J. Vleugels, E. W. Meijer, A. R. A. Palmans, P. Zijlstra and L. Albertazzi, *J. Am. Chem. Soc.*, 2024, **146**, 19974–19985.
75 J. Ihli, D. C. Green, C. Lynch, M. A. Holden, P. A. Lee, S. Zhang, I. K. Robinson, S. E. D. Webb and F. C. Meldrum, *Angew. Chem., Int. Ed.*, 2019, **58**, 17328–17334.
76 S. Letschert, A. Göhler, C. Franke, N. Bertleff-Zieschang, E. Memmel, S. Doose, J. Seibel and M. Sauer, *Angew. Chem., Int. Ed.*, 2014, **53**, 10921–10924.
77 D. Nair, E. Hosy, J. D. Petersen, A. Constals, G. Giannone, D. Choquet and J. B. Sibarita, *J. Neurosci.*, 2013, **33**, 13204–13224.
78 N. Ehmann, S. Van De Linde, A. Alon, D. Ljaschenko, X. Z. Keung, T. Holm, A. Rings, A. DiAntonio, S. Hallermann, U. Ashery, M. Heckmann, M. Sauer and R. J. Kittel, *Nat. Commun.*, 2014, **5**, 4650.
79 J. Yoo and Y. Y. Won, *ACS Biomater. Sci. Eng.*, 2020, **6**, 6053–6062.
80 Y. H. Yun, B. K. Lee and K. Park, *J. Controlled Release*, 2015, **219**, 2–7.
81 Y. W. Lim, W. S. Tan, K. L. Ho, A. R. Mariatulqabtiah, N. H. A. Kasim, N. A. Rahman, T. W. Wong and C. F. Chee, *Pharmaceutics*, 2022, **14**, 614.
82 L. Pourtalebi Jahromi, M. Ghazali, H. Ashrafi and A. Azadi, *Heliyon*, 2020, **6**, e03451.

